Interpretation of the Acoustic Black Hole effect based on the concept of critical coupling

J. Leng[a], A. Pelat[a], R. Picó[b], J.-P. Groby[a], V. Romero-García[a], F. Gautier[a]

[a] *Laboratoire d'Acoustique de l'Université du Mans, LAUM, UMR CNRS 6613, Av. Olivier Messiaen, Le Mans, France*
[b] *Instituto para la Gestión Integral de zonas Costeras (IGIC), Universitat Politècnica de València, Paranimf 1, 46730, Gandia, Spain*

Abstract

An Acoustic Black Hole (ABH) is a passive vibration damping device based on a local reduction of the thickness associated to a thin layer of attenuating material. This work aims at theoretically revisit the ABH effect by analyzing the ABH trapped modes in the complex frequency plane. This analysis relies on an analytical model based on the one-dimensional thin beam theory and the transfer matrix method assuming that the ABH termination is discretized by constant thickness piecewise elements. The model is validated against numerical simulations by the Finite Element Method. The reflection coefficients of several ABH terminations are studied. The results show that an ABH presents an infinite number of modes associated to an infinite number of poles and zeros, the density and quality factor of which depend on the order of the ABH profile. Therefore, the damping efficiency of the ABH termination results from a balance between the energy leakage of each mode and the added losses. In particular, the broadband absorption of the vibration energy is achieved for frequencies higher than the one of the mode that is critically coupled due to the low quality factor of the poles and zeros. This type of analysis is used to interpret the ABH effect. It provides the optimised damping needed to obtain critical coupling condition, and is suitable for the optimization of one-dimensional ABH terminations.

Keywords: vibration damper, Acoustic Black Hole effect, reflection coefficient, critical coupling

1. Introduction

Vibration damping of mechanical structures at low frequencies is a crucial issue in terms of safety, stability, and comfort in many industrial applications. The usual passive way to solve this problem relies on the use of viscoelastic coatings [1]. In this case, the vibration damping results from heat dissipation obtained with the shear forces in the viscoelastic material. Nevertheless, this solution may be accompanied by a significant increase in the structure weight which becomes inconvenient for obvious practical,ecological and economic reasons. The use of the Acoustic Black Hole (ABH) is therefore particularly relevant in this context. The ideal implementation of an ABH in an one-dimensional (1D) beam consists of continuously decreasing the beam thickness according to a power-law till it vanishes [2]. As a result, the flexural wave slows down by propagating along the termination until reaching zero phase and group velocities at its extremity. The wave is therefore not reflected and an anechoic termination is obtained. However, in practice the thickness profile must be truncated. This leads to a non-null thickness at its tip and therefore to a total reflection of the flexural waves in the absence of loss. However, losses are not avoidable, and combining the ABH effect and the presence of losses damping devices has been proposed as spiral ABHs [3], compound ABHs [4], and ABHs resonant beam damper [5]. Other kind of applications as insulating [6] and lensing [7] devices have been also proposed.

Recently, the representation of the eigenvalues of the scattering matrix in the complex frequency plane has been exploited to interpret and design perfect absorbers [8, 9]. In the case of a locally resonant termination, for instance an ABH termination, these eigenvalues are given by the reflection coefficient. It has been shown that the reflection coefficient presents pairs of zeros and poles in the complex frequency plane. These zeros and poles are complex conjugate one with respect to the other in the lossless case, thus being symmetric with respect to the real frequency plane. In the ideal case of an ABH in which the thickness is zero, the reflection coefficient should present a continuous of poles and zeros

that coalesce at the real frequency axis. However, this situation is not realistic since the thickness, despite its small value, is nonetheless always finite. In this case, infinite discrete symmetric pairs of poles and zeros appear in the complex frequency plane. At this stage, it is worth noting that the imaginary part of the pole represents the energy leakage between the ABH tip and the main beam as this kind of terminations can be interpreted as open resonators [9].

The damping efficiency of these open resonators can be improved by making use of the inherent losses of the system. In doing so, for instance by taping a layer of viscoelastic material along the thickness profile [9], the zero and poles can be tuned in the frequency plane. Thus, as the loss increases the pair zero/pole moves along the imaginary frequency axis in the same direction, locating the zeros closer to the real frequency axis. In particular, perfect absorption of the incident wave can be achieved when the zero is located on the real frequency axis, or physically when the energy leakage is perfectly compensated by the added losses. This corresponds to the critical coupling condition [10]. This has been widely used to design perfect absorbers in various fields of wave physics [11, 12, 13]. Concurrently, it has been shown that the damping efficiency of a practical ABH, also called ABH effect, can be significantly improved also by adding a thin layer of viscoelastic material along the ABH profile [14, 15]. The reflection coefficient of such a system has been studied both experimentally [16] and numerically by using various methods: plane wave decomposition [17] or multimodal approaches [18], Finite Difference [19] or Finite Element [20] methods, and wavelet decomposition [21] to cite a few. In general, the ABH effect is characterized by drops of the reflection coefficient at specific frequencies corresponding to modes of the tapered zone [19]. However, it has not been shown in detail how the losses have to be managed to obtain the perfect absorption of flexural waves.

This article reports on this link between the complex nature of the trapped modes within a 1D ABH and its reflection coefficient drops, in terms of depth and frequency width. More specifically, the purpose of the present article is to analyse first the absorbing efficiency of the ABH by using the critical coupling

condition which has been recently introduced to analyze the damping of flexural waves [9]. The absorption of the ABH termination can be controlled by tuning the losses introduced via the added viscoelastic coating and the geometry of the ABH. Two strategies to optimize the absorption efficiency of an ABH termination at low frequency are then proposed, both consisting in applying the critical coupling condition. The first consists in tuning the losses introduced by the viscoelastic layer by shaping its thickness profil in order to achieve the critical coupling condition at several resonances of the ABH. The second strategy is based on the addition of a mass at the extremity of the ABH which decreases the first resonance frequency of the ABH. The critical coupling is then applied at this specific frequency to obtain a low frequency absorption by the termination.

The analyzed system is composed of a main beam terminated by open resonator which corresponds to an ABH of finite length. The ABH termination is discretized by constant thickness piecewise elements. A thin viscoelastic coating is also attached to the ABH creating a composite material. This composite material is modeled with the Ross-Kerwin-Ungar (RKU) method [1]. The vibration response of the composite ABH is studied by means of the transfer matrix method (TMM) [22]. In particular, the eigenvalue of the scattering matrix, S, for the propagating waves are analyzed in the complex frequency plane [8, 9], providing insightful interpretation on the absorption efficiency of the ABH.

The work is organized as follows. In Section 2, the theoretical model used to analyze the reflection of flexural wave by a profiled termination is presented for a 1D reflection problem. In Section 3, the physical interpretations of the ABH effect of a truncated ABH with a coating layer by using the complex frequency plane in the lossless and lossy cases are presented. Section 4 proposes two strategies to optimize the absorption efficiency of an ABH termination at low frequency. The first consists in tuning the losses introduced by the added coating layer in order to apply the critical coupling condition. The second strategy consists in adding a mass at the end of the ABH in order to introduce a degree of freedom in the low frequency regime, where the ABH is not efficient. All the analytical results are validated against a numerical model using finite

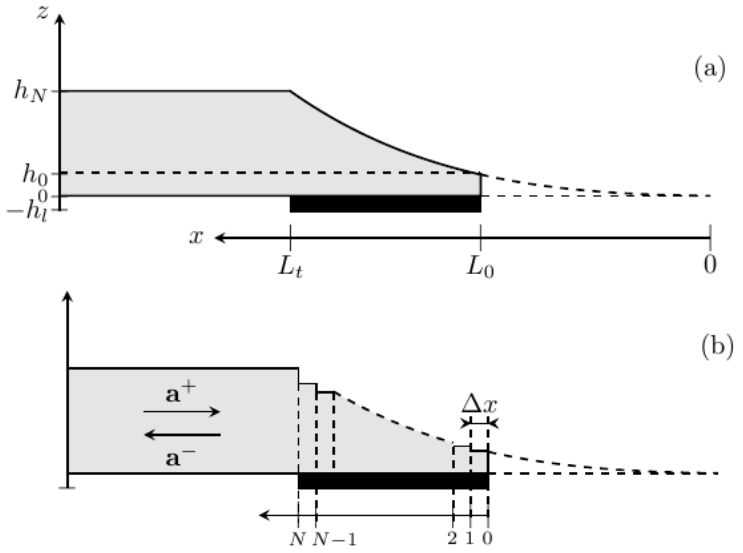

Figure 1: (a) Diagrams of the 1D reflection problem for flexural waves. (b) Spatial discretisation of the thickness profil of the ABH termination.

element formalism. Finally, Section 5 summarizes the main results and gives the concluding remarks.

2. Theoretical model for the reflection of flexural waves by a profiled termination

This Section describes the theoretical model used to study the absorption of flexural waves by a 1D open, lossy, and profiled termination. The model is based on the TMM as proposed by Mace [22] and previously used to interpret the perfect absorption of flexural waves of a termination composed of a thin connected beam of uniform thickness [9]. This method is applied here to calculate the reflection coefficient of semi-infinite beam terminations described by $N-1$ piecewise constant property profiles, as depicted in Fig. 1.

2.1. Reflection problem

Consider a time harmonic ($e^{i\omega t}$) incident plane wave that impinges the ABH termination from the left (see Fig. 1(a)). The ABH is discretized into $N-1$ beams of identical length Δx, but of height h_j, bending stiffness $D_j = EI_j$ where $I_j = bh_j^3/12$ denotes the second moment of area, b being the beam width, and wavenumbers $k_j^4 = \dfrac{\rho_j h_j \omega^2}{D_j}$, $j = 0, ..., N$ (see Fig. 1(b)). The material of the main beam and the uncoated ABH termination is identical, with E its Young's modulus and ρ its density. The losses are accounted for via a loss factor η, the Young's modulus thus being $E = E(1 + i\eta)$. The possible variations of the loss factor against the frequency are ignored in this study, and η is assumed yo be constant. This assumption is reasonnable in the case of the aluminium beam studied in this paper. The continuity and equilibrium of the displacement, slope, bending moment and shear force are considered at the interfaces between each consecutive beams. Assuming the Euler-Bernoulli conditions, the flexural displacement $\mathbf{w}$ in the main beam, i.e., for $x > L_t$, reads as

$$\mathbf{w} = \mathbf{a}^+ + \mathbf{a}^- = (\mathbf{I} + \mathbf{R_N}) \cdot \mathbf{a}^+, \tag{1}$$

where $\mathbf{a}$ are the complex amplitude vectors of the propagative and evanescent waves, the signs $^+$ and $^-$ denote the ingoing and outgoing waves respectively, $\mathbf{R_N}$ is the reflection matrix at $x = L_t$, i.e. at the interface between the main beam and the ABH termination, and $\mathbf{I}$ is the identity matrix.

The expression of $\mathbf{R_N}$ is a combination of reflection and transmission matrices at the interfaces of all the discrete beams that form the termination. It is obtained iteratively starting from the reflection matrix of the free termination $\mathbf{R_0} = \mathbf{r_{free}}$ given by

$$\mathbf{r_{free}} = \begin{bmatrix} -\imath & (1+\imath) \\ (1-\imath) & \imath \end{bmatrix}. \tag{2}$$

The iterative scheme takes the following form [22]

$$\mathbf{R_j} = \mathbf{r_{j-1,\,j}} + \mathbf{t_{j-1,\,j}}(\mathbf{f_{j-1}}\mathbf{R_{j-1}}\mathbf{f_{j-1}})^{-1} - \mathbf{r_{j,\,j-1}})^{-1}\mathbf{t_{j,\,j-1}}, \text{for } j = 1 \text{ to } N, \tag{3}$$

where $\mathbf{r_{i,j}}$ and $\mathbf{t_{i,j}}$ are the reflection and transmission matrices from section i to section j respectively. Considering the continuity and equilibrium of the displacement, slope, bending moment and shear force, these matrices are given by

$$\mathbf{t_{ij}} = \frac{4}{\Delta_{ij}} \begin{bmatrix} (1+\beta_{ij})(1+\gamma_{ij}) & (-1+i\beta_{ij})(1-\gamma_{ij}) \\ (-1-i\beta_{ij})(1-\gamma_{ij}) & (1+\beta_{ij})(1+\gamma_{ij}) \end{bmatrix}, \tag{4}$$

$$\mathbf{r_{ij}} = \frac{2}{\Delta_{ij}} \begin{bmatrix} -2(\beta_{ij}^2-1)\gamma_{ij} - i\beta_{ij}(1-\gamma_{ij})^2 & (1+i)\beta_{ij}(1-\gamma_{ij}^2) \\ (1-i)\beta_{ij}(1-\gamma_{ij}^2) & -2(\beta_{ij}^2-1)\gamma_{ij} + i\beta_{ij}(1-\gamma_{ij})^2 \end{bmatrix}, \tag{5}$$

where $\beta_{ij} = \dfrac{k_j}{k_i}$ and $\gamma_{ij} = \dfrac{D_j k_j^2}{D_i k_i^2}$ correspond to the ratios of wavenumbers and bending wave impedances, and $\Delta_{ij} = (1+\beta_{ij})^2(1+\gamma_{ij})^2 - (1+\beta_{ij}^2)(1-\gamma_{ij})^2$. The diagonal transfer matrix in the uniform beams $\mathbf{f_j}$ is expressed as

$$\mathbf{f_j} = \begin{bmatrix} e^{-ik_j x} & 0 \\ 0 & e^{-k_j x} \end{bmatrix}. \tag{6}$$

$\mathbf{R_N}$ is thus a 2×2 matrix where the upper diagonal component corresponds to the reflection coefficient of the propagative wave. The study focuses on the term $R_N = \mathbf{R_N}(1,1)$ that is the only one related to the carried energy. Only $\mathbf{R_N}(1,1)$ and $\mathbf{R_N}(2,1)$ contribute to the reflected field in the abscence of evanescent incident wave. Moreover, $\mathbf{R_N}(2,1)$ vanishes in the far-field ($x \to -\infty$), as it corresponds to converted wave from the propagative to evanescent ones during the reflexion process. The absorption coefficient α_R can thus be written as:

$$\alpha_r = 1 - |R_N|^2, \qquad x \to -\infty. \tag{7}$$

2.2. Introducing viscoelastic losses in the system: the RKU model

A thin viscoelastic layer of identical material, and constant thickness piecewise h_j^l is now added all along the termination length as shown in Fig. 1. Each discretized element of the viscoelastic layer coincides with those of the ABH. The losses are assumed to be frequency independent and characterized by a

Young Modulus $E_l(1+i\eta_l)$, where η_l is the loss factor of the viscoelastic material. Using the RKU model [1], the effective bending stiffness D_j^c of the j-th discretized composite beam of the coated tapered area is written as [17]:

$$D_j^c = EI_j \left[(1+i\eta) + e_c \tilde{h}_c^3 (1+i\eta_l) + \frac{3+(1+\tilde{h}_c)^2 e_c h_c [1-\eta\eta_l + i(\eta+\eta_l)]}{1+e_c\tilde{h}_c(1+j\eta_l)} \right], \tag{8}$$

where the indices j and l stand for the parameters of the uncoated j-th beam of the termination and the absorbing layer respectively, $e_c = E_l/E$ and $\tilde{h}_c = h_j^l/h_j$. In addition, the wave number k_j^c of the j-th composite beam satisfies $(k_j^c)^4 = \dfrac{\rho_j^c h_j^c \omega^2}{D_j^c}$, where $h_j^c = h_j^l + h_j$ is the total composite height and $\rho_j^c = (\rho_j h_j + \rho_l h_l)/h_j^c$ is the density.

3. Interpretation of the ABH effect by analyzing R_N in the complex frequency plane

The absorption of flexural waves by a discretized 1D ABH termination coated by a viscoelastic layer is now analyzed in the reflection problem. In this section, the thickness h_j^l of the viscoelastic layer is considered constant such that $h_j^l = h_l$, for $j = 0, ..., N-1$. The eigenvalue of the scattering matrix of the propagative wave reduces to R_N in the current case and is analyzed in the complex frequency plane[8, 9]. The material properties and geometric parameters are also given in table 1.

3.1. Analysis of lossless ABH terminations with different thickness profiles.

Four configurations of termination with different thickness profiles of the uncoated ABH are analyzed in this paragraph. The four thickness profiles differ one another by their power-law χ such that each profile equation reads as :

$$h(x) = h_N \left(\frac{x}{L_t} \right)^{\chi}, \forall x > L_0. \tag{9}$$

The analyzed orders are linear ($\chi = 1$), quadratic ($\chi = 2$), cubic ($\chi = 3$) and quartic ($\chi = 4$) respectively and are depicted in Fig. 2(d). The reflection

	Geometric parameters	Material parameters
Main beam	$h_N = 5$ mm $b = 2$ cm	$\rho = 2700$ kg.m^{-3} $E = 70$ GPa η
Acoustic Black Hole	$h_0 = 0.1125$ mm $b = 2$ cm $L_t = 20$ cm $L_0 = 3$ cm $N = 201$	ρ_j D_j
Coating layer	$h_l = 0.7$ mm	$E_l = 0.5 \times 10^{-3}$ GPa $\rho_l = 950$ kg.m^{-3} η_l

Table 1: Geometric and material parameters of the studied systems. The value of the loss factors η and η_l depends on the experimental set-up used. The parameter b corresponds to the width of the system.

problem is analyzed first for each configuration in the lossless case. In this case, no dissipation is considered and Young moduli are pure real ($\eta = \eta_l = 0$). $\log_{10}(|R_N|)$ of the different thickness profiles are depicted in Fig. 2(a)-(d). For each profil order, the poles and zeros are symmetric by pair with respect to the real frequency axis in the lossless case, i.e. the complex frequencies associated to one pair of pole and zero are complex conjugate one from the other. This symmetric distribution comes from the time invariance symmetry of the scattering matrix [8]. The pole frequencies correspond to the resonances of the ABH termination while the zero frequencies correspond to destructive interference phenomena. The value of $|R_N|$ along the real frequency axis is equal to 1 as expected since no energy is lost in the system and the incoming wave is completely reflected back (see Fig. 2(d)). Since the ABH terminations are open resonators, the imaginary part of the poles in the lossless case represents the amount of energy leaked by the resonator through the main beam [8]. The quality factor of the resonances can be given by $Q = \frac{\mathrm{Im}(\omega_p)}{2\mathrm{Re}(\omega_p)}$ where ω_p is the

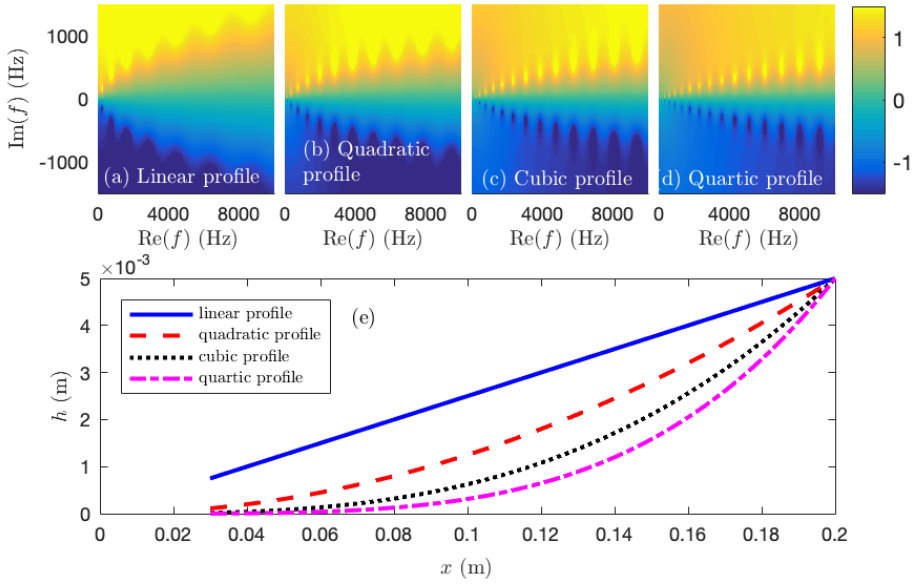

Figure 2: (a)-(d) Representation of $\log_{10}(|R_N|)$ in the complex frequency plane for different thickness profiles of ABH in the lossless case (linear, quadratic, cubic and quartic thickness profiles respectively). (e) Thickness profiles of the ABH studied in (a)-(d).

complex frequency of the pole [8].

By observing the general trend of the discret distribution of poles and zeros: it is possible to note that the imaginary part of the poles (and zeros) increases (decreases) when the real part of the frequency increases, meaning that more energy leaks out through the resonator when the frequency increases and therefore the quality factor of the resonance decreases as the frequency increases. However the value of the quality factor depends on the analyzed profile. Of particular interest is the increase of the quality factor of the modes, as well as the increase of the density of poles for profiles with higher order as shown in Figs. 2(a)-(d). The imaginary part of the frequency for a given zero is closer to the real frequency axis as the order of the profile increases, meaning that the quality factor is higher and the mode is more trapped in the termination with bigger order profile. The energy leakage is therefore lower for higher order

profiles. As the imaginary frequency of the pole decreases, the quality factor Q increases, leading to narrower poles and thus zeros.

The previous analysis corresponds to the lossless case. The next stage is to introduce losses in order to shift the zeros to the real frequency axis and design efficient absorbing materials. The first step consists in choosing the best profile. To do that, a compromise between the density of poles and the quality factor should be obtained. In fact, if a low (high) order profile is chosen, the density of poles will be low (high) and the quality factor will be low (high), requiring big (low) amount of losses to produce a rippled absorption spectrum with broad (narrow) absorption ripples. The quadratic profile is chosen here, with $\chi = 2$ which shows a reasonable density of poles with a leakage that can be compensated by realistic materials as the one used in [9].

3.2. Lossy case.

Losses are now introduced into the system by adding an imaginary part to the Young modulus of the damping material of the viscoelastic coating such that it reads as $E_l(1+i\eta_l)$. Losses in the uncoated termination and the main beam are neglected, $\eta = 0$. In doing so, the symmetry between the poles and zeros with respect to the real frequency axis is broken [8]. Figs. 3(b)-(c) depict $\log_{10}(|R_N|)$ in the complex frequency plane for two different values of η_l, which have to be compared to the lossless case depicted in Fig. 3(a) ($\eta_l = 0$). As the losses induced by the damping layer increase ($\eta_l = 2$ in Fig. 3(b) and $\eta_l = 4$ in Fig. 3(c)), the zeros move to the real frequency axis. Drops of $|R|^2$ appear therefore in Fig. 2(d) associated to the resonance frequencies of the ABH termination. The closer to the real frequency axis the zero in the complex frequency plane, the greater the drop of $|R|^2$ with respect to the real frequency with two distinct situations: either the zeros are located in the opposite half space of the poles and losses lack, or the zeros are located in the same half space as the poles and losses exceed. When the amount of losses exactly compensates the leakage of the system, the corresponding zero of the reflection coefficient is located on the real frequency axis, e.g. at Re(f)=3108 Hz in Fig. 3(b). This situation is known as the critical

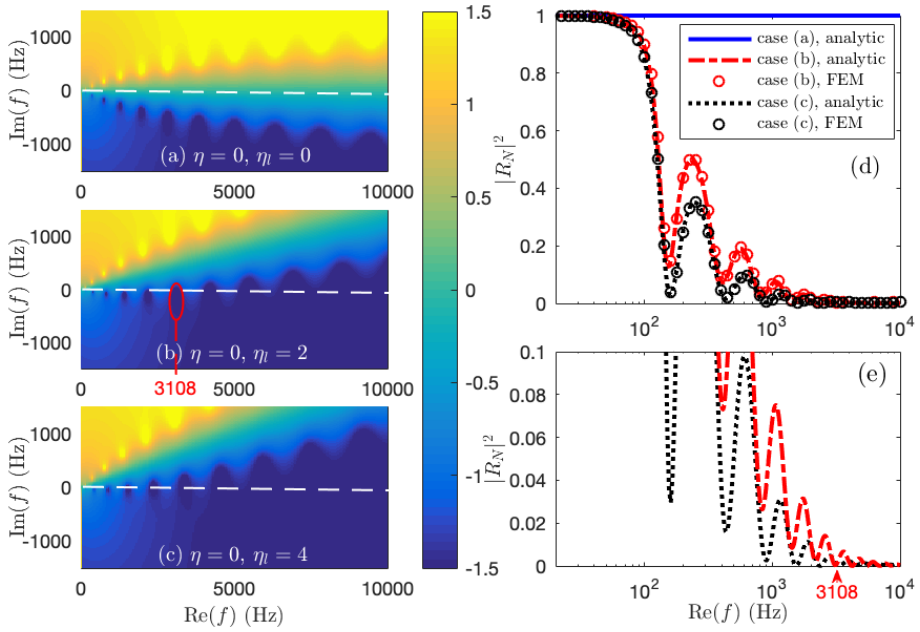

Figure 3: (a)-(c) Representation of $\log_{10}(|R_N|)$ in the complex frequency plane for different values of loss factor of the beam η and the viscous layer η_l. (d) Blue continuous, red dash-dotted and black dotted lines show the analytical reflection coefficient according to the real frequency for the configuration of (a),(b) and (c) respectively. Black and red circles show the numerical validations of configuration (b) and (c) respectively. (e) Zoom of the analytical curves of (d).

coupling condition [10] and implies the impedance matching between the main beam and the resonator, leading to a perfect absorption of the incident wave at this specific real frequency (see Fig. 3d).

An overlapping of the zero width on the real frequency axis is observed in Fig. 3(b) above the frequency for which the coupling condition is satisfied (3108Hz). This is due to the geometry of the resonator that leads to low quality factor resonances. The overlapping of the wide zeros results in a broadband quasi-perfect absorption and $|R_N|^2 \simeq 0$ in this frequency range (see Fig. 3(d)). This result is one interpretation of the ABH effect at high frequency and is the main contribution of this paper. The damping effect of a truncated ABH is a consequence of the critical coupling at one resonance frequency of the ABH

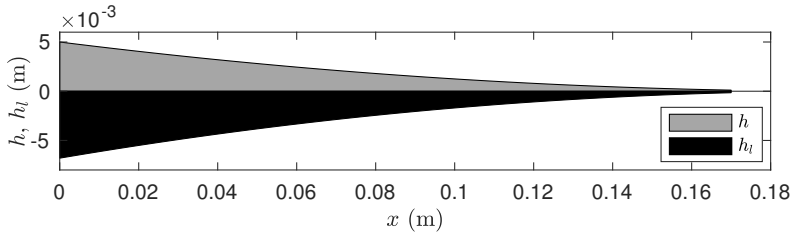

Figure 4: Thickness profile of the ABH termination (grey) and the coating layer (black).

and the broadband quasi-perfect absorption at higher frequencies. For practical application, one interesting goal is to design a critically coupled system at the lowest resonance as possible. However, this may require a huge amount of losses, therefore increasing the mass of the system, possibly destroying the higher frequency efficiency. Other strategies should therefore be developed.

4. Enhancement of the absorption of an ABH termination.

This section proposes methods to enhance the absorption performance of an ABH termination. These methods are based on the use of the complex frequency plane, and can also be applied to any geometry of termination. Two methods are presented. The first one is based on the spatial distribution of the losses introduced by the coating layer by gradually changing its thickness, i.e. h_j^l is also varying with h_j, $j = 0, ..., N-1$. The second one consists in slightly modifying the geometry of the ABH, by adding a mass at the termination end. In this case, the critical coupling at the first zero of the termination may be obtained, leading to a perfect absorption at low frequency.

4.1. Tuning the losses introduced by the coating layer

An enhancement of the absorption properties of an ABH is proposed through tuning the distribution of losses along the ABH termination. Except for the thickness of the coating layer, the geometric and material parameters of the ABH and the coating layer remain the same in this study as in the previous sections (see Table 1).The thickness profile of the coating layer is shaped so

that the losses introduced in the system efficiently compensate the leakage for each resonance of the termination, producing a broadband absorption. The progressive variation of losses is based on a similar phenomenon to graded materials [23]. The incoming wave reduces its speed progressively as it propagates through the ABH. The thickness of the coating layer (and thus the amount of losses) is tapered in such a way that the losses are higher where the wave travels faster. The thickness profile of the coating layer therefore decreases as well as the one of the beam as depicted in Fig. 4 and it is defined as:

$$h_l(x) = 1.36 \times h_0 \left(\frac{x}{L_t}\right)^2, \forall x > L_0. \tag{10}$$

Figs. 5(a)-(b) show the reflection coefficient of the ABH and the coating layer described in Fig. 4 in the complex frequency plane in the lossless ($\eta = 0$, $\eta_l = 0$) and lossy ($\eta = 0$, $\eta_l = 2$) cases respectively. As the losses are introduced, the set of zeros are all aligned on the real frequency axis. The critical coupling is therefore performed for each resonance frequency in the analyzed frequency band, leading to a total absorption of flexural waves at these particular frequencies. In order to compare, Fig. 5(c)-(d) depict the reflection coefficient of the ABH with a coating layer of constant thickness $h_l = 4.7$ mm in the complex frequency plane in the lossless ($\eta = 0$, $\eta_l = 0$) and the lossy cases ($\eta = 0$, $\eta_l = 2$) respectively. Both configurations are designed in such a way that they provide the same absorption performance at the first resonance frequency $f_0 = 185.2$ Hz of the termination in the lossy case. It is worth noting that the quality factor and the density of poles depend on the profile of the coating layer: the uniform coating layer provides smaller density of poles and smaller quality factors than the profiled one. However larger zeros in the complex frequency plane are present for the uniform profile (see Fig. 5(d)).

Contrary to the profiled case, the uniform one produces a distribution of large zeros that are not aligned in the real frequency axis, so without perfect absorption peaks. In the case of the uniform coating layer, the control of the position of a given zero cannot be achieved independently from the others since

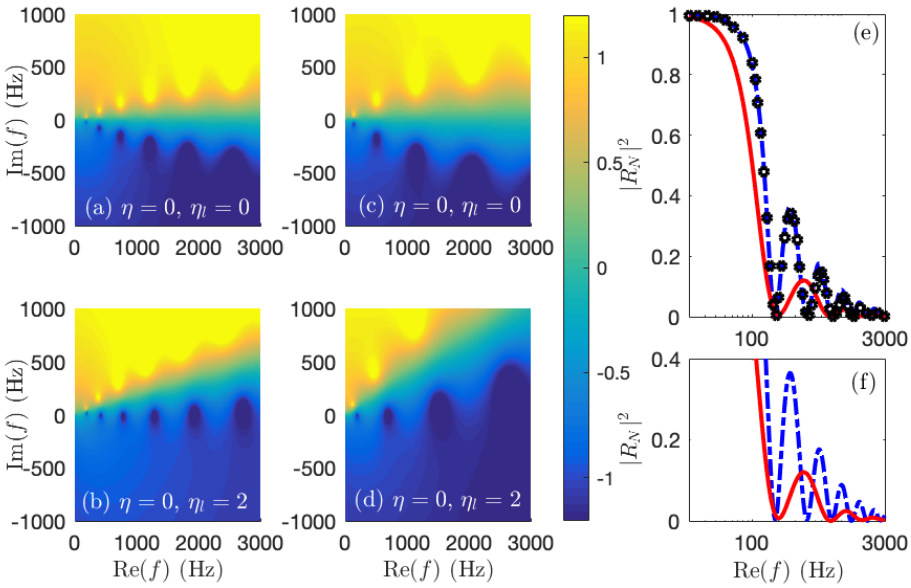

Figure 5: (a)-(b) Representation of $\log_{10}(|R_N|)$ of the ABH with the profiled coating layer in the complex frequency plane for the lossless ($\eta = 0$, $\eta_l = 0$) and lossy ($\eta = 0$, $\eta_l = 2$) case respectively. (c)-(d) Representation of $\log_{10}(|R_N|)$ of the ABH with a coating layer of constant thickness ($h_l = 4.7$ mm) in the complex frequency plane for the lossless ($\eta = 0$, $\eta_l = 0$) and lossy ($\eta = 0$, $\eta_l = 2$) case respectively. (e) Blue dash-dotted line and black circles show the reflection coefficient of the ABH with a profiled coating layer according to the real frequencies. Red line shows the analytical reflection coefficient of the ABH with a coating layer of constant thickness ($h_l = 4.7$ mm). (f) Zoom of the analytical curves of (e).

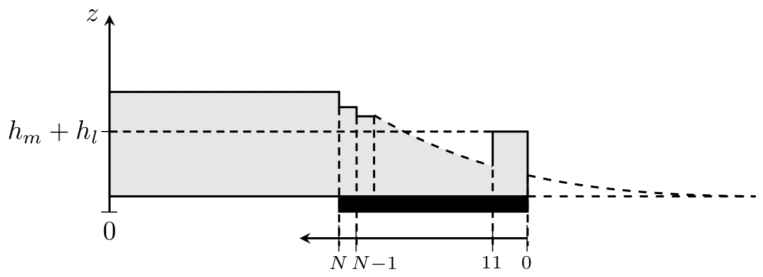

Figure 6: Diagram of the spatial discretisation of the ABH with an added mass.

the introduced losses are frequency independent in the model, but also since the thickness and η_l are constant (see also Figs. 5(c)-(d)). Furthermore, all the zeros are aligned in the real frequency axis in the profiled coating as shown in Figs. 5(a)-(b). This result highlights how a profiled coatings can be used to produce a cascade of perfect absorption peaks. In order to highlight this point, the reflection coefficients of these two types of ABH terminations are shown in Fig. 5(e). The profiled case shows several peaks with perfect absorption while the uniform profile has peaks with lower quality factors.

4.2. ABH termination with an added mass

Another parametric analysis based on the complex frequency plane is proposed to improve the absorbing performance of the ABH at low frequencies. The study is carried out by modifying the geometry of the ABH. In particular, a mass is added at the termination end with a varying thickness. The thickness h_m of the mass varies from 0.2 mm to 5 mm. The termination+beam system is still discretized by $N = 201$ beams and the mass consists of increasing the thickness of the 11 first beams of the termination (see Fig. 6). The geometric and material parameters of the ABH and the coating layer remain the same as in the previous section and are described in Tab. 1. The lossy case is considered here and $\eta = 0$ and $\eta_l = 2$.

Fig. 7(a) depicts the reflection coefficient around its first zero in the complex frequency plane for an ABH configuration without added mass. The path of the zero in the complex frequency plane is also depicted according to the increase

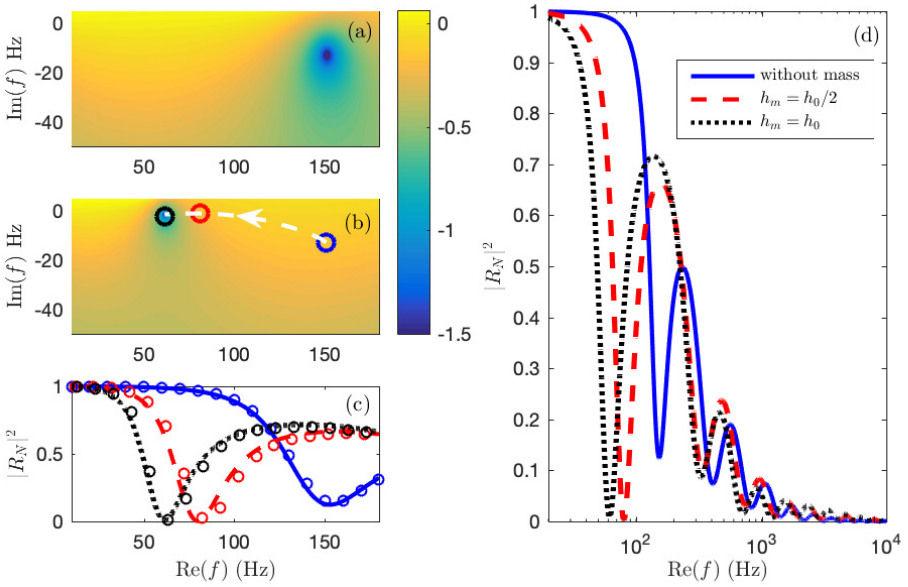

Figure 7: (a) Representation of $\log_{10}(|R_N|)$ for the ABH in the complex frequency plane around its first zero. (b) Representation of $\log_{10}(|R_N|)$ in the complex frequency plane around its first zero in the case with an added mass of thickness $h_m = h_l$. White dashed line corresponds to the path of the zero when the thickness of the mass is increased. Blue, red and black circles give the positions of the zero for the configurations ABH ($h_m = h_t$), $h_m = h_0/2$ and $h_m = h_0$ respectively. (c) Blue continuous, red dashed and black dotted lines show the analytical reflection coefficient around the first real resonance frequency for the configurations shown with circles of same color in (b). Blue, red and black circles show the numerical validations. (d) Blue continuous, red dashed and black dotted lines show the analytical reflection coefficient according to the real frequency for the configurations shown with circles of same color in (b).

of the mass thickness in Fig. 7(b). As the mass thickness increases, the added mass effect in the termination increases too and the real frequency of the zero decreases. Moreover, the zero moves to the real frequency axis as the mass thickness increases. This is due to a localisation of the mode in the termination, leading to a decrease in leakage and thus a decrease in the absolute value of the imaginary frequency of the zero. In particular, the zero of the reflection coefficient is located on the real frequency axis starting from $h_m = h_N/2$. The critical coupling is therefore obtained and a perfect absorption of the incident wave is observed at $\mathrm{Re}(f) = 80$ Hz and $\mathrm{Re}(f) = 61.5$ Hz for $h_m = h_N/2$ and $h_m = h_N$ respectively (see Fig. 7(c)). It is worth noting that the addition of mass does not deteriorate the absorbing properties of the ABH at high frequencies as seen in Fig. 7(d). These results highlight the possibility to improve the absorption efficiency of an 1D termination by modifying its geometry and by analyzing the position of the zeros of its reflection coefficient in the complex frequency plane.

5. Conclusions

Absorption of propagative flexural waves by means of an 1D ABH termination is analyzed in this work in the case of a reflection problem. The ABH effect is interpreted through the use of the complex frequency plane. The positions of the zeros of the eigenvalues of the scattering matrix in the complex frequency plane provide informations on the absorption properties of the ABH. The ABH effect may be interpreted as a consequence of the critical coupling at one resonance frequency of the ABH and of the broadband quasi-perfect absorption at higher frequencies, thanks to the specific geometry of the resonator. This point is the main conclusion of the paper since it provides a physical explanation of the ABH efficiency. The understanding of this mechanism provides the keys to the optimisation procedure of an absorbing termination. Two methods are proposed to improve the absorption of a 1D ABH. The first consists in tuning the losses introduced in the system by shaping the thickness profile of the coating

layer. In doing so it is possible to control the losses introduced in the resonator according to the real frequency. The second method relies on the addition of a mass at the end of the ABH. The configuration of perfect absorption at the first resonance frequency of the resonator can be obtained and controlled according to the added mass by controlling the position of the corresponding zero in the complex frequency plane.

Acknowledgements

This work has been founded by the RFI Le Mans Acoustic (Région Pays de la Loire) within the framework of the Metaplaque project. This article is based upon work from COST action DENORMS CA 15125 , supported by COST (European Cooperation in Science and Technology). This work was partly supported by the Spanish Ministry of Economy and Innovation (MINECO) and European Union FEDER through project FIS2015-65998-C2-2 and by project AICO/2016/060 by Consellería de Educación, Investigación, Cultura y Deporte de la Generalitat Valenciana. it was also supported by the project eTNAA (projet ANR 2017-2010).

References

References

[1] D. Ross, E. Ungar, E. Kerwin., Damping of plate flexural vibrations by means of viscoelastic laminae, Structural damping (1960) 49–87.

[2] M. Mironov, Propagation of a flexural wave in a plate whose thickness decreases smoothly to zero in a finite interval, Soviet Physics Acoustics-USSR 34 (3) (1988) 318–319.

[3] J. Y. Lee, W. Jeon, Vibration damping using a spiral acoustic black hole, The Journal of the Acoustical Society of America 141 (3) (2017) 1437–1445.

[4] T. Zhou, L. Tang, H. Ji, J. Qiu, L. Cheng, Dynamic and static properties of double-layered compound acoustic black hole structures, International Journal of Applied Mechanics 9 (05) (2017) 1750074.

[5] T. Zhou, L. Cheng, A resonant beam damper tailored with acoustic black hole features for broadband vibration reduction, Journal of Sound and Vibration 430 (2018) 174–184.

[6] A. Climente, D. Torrent, J. Sánchez-Dehesa, Omnidirectional broadband insulating device for flexural waves in thin plates, Journal of Applied Physics 114 (21) (2013) 214903.

[7] A. Climente, D. Torrent, J. Sánchez-Dehesa, Gradient index lenses for flexural waves based on thickness variations, Applied Physics Letters 105 (6) (2014) 064101.

[8] V. Romero-García, G. Theocharis, O. Richoux, V. Pagneux, Use of complex frequency plane to design broadband and sub-wavelength absorbers, J. Acoust. Soc. Am. 139 (6) (2016) 3395–3403.

[9] J. Leng, F. Gautier, A. Pelat, R. Picó, J.-P. Groby, V. Romero-García, Limits of flexural wave absorption by open lossy resonators: reflection and transmission problems, New J. Phys. 21 (053003).

[10] A. Yariv, Universal relations for coupling of optical power between microresonators and dielectric waveguides, Electron. Lett. 36 (4) (2000) 321–322.

[11] J. R. Piper, S. Fan, Total absorption in a graphene monolayer in the optical regime by critical coupling with a photonic crystal guided resonance, Acs Photonics 1 (4) (2014) 347–353.

[12] N. Jiménez, V. Romero-García, V. Pagneux, J.-P. Groby, Rainbow-trapping absorbers: Broadband, perfect and asymmetric sound absorption by subwavelength panels for transmission problems, Sci. Rep. 7 (1) (2017) 13595.

[13] J.-P. Groby, R. Pommier, Y. Aurégan, Use of slow sound to design perfect and broadband passive sound absorbing materials, J. Acoust. Soc. Am. 139 (4) (2016) 1660–1671.

[14] V. Krylov, F. Tilman, Acoustic 'black holes' for flexural waves as effective vibration dampers, Journal of Sound and Vibration 274 (3-5) (2004) 605–619.

[15] V. V. Krylov, R. Winward, Experimental investigation of the acoustic black hole effect for flexural waves in tapered plates, Journal of Sound and Vibration 300 (1-2) (2007) 43–49.

[16] V. Denis, F. Gautier, A. Pelat, J. Poittevin, Measurement and modelling of the reflection coefficient of an acoustic black hole termination, Journal of Sound and Vibration 349 (2015) 67–79.

[17] V. Georgiev, J. Cuenca, F. Gautier, L. Simon, V. Krylov, Damping of structural vibrations in beams and elliptical plates using the acoustic black hole effect, Journal of sound and vibration 330 (11) (2011) 2497–2508.

[18] V. Denis, A. Pelat, F. Gautier, Scattering effects induced by imperfections on an acoustic black hole placed at a structural waveguide termination, Journal of Sound and Vibration 362 (2016) 56–71.

[19] V. Denis, A. Pelat, F. Gautier, B. Elie, Modal overlap factor of a beam with an acoustic black hole termination, Journal of Sound and Vibration 333 (12) (2014) 2475–2488.

[20] P. A. Feurtado, S. C. Conlon, Investigation of boundary-taper reflection for acoustic black hole design, J. Noise Cont. Eng. 63 (5) (2015) 460.

[21] L. Tang, L. Cheng, H. Ji, J. Qiu, Characterization of acoustic black hole effect using a one-dimensional fully-coupled and wavelet-decomposed semi-analytical model, Journal of Sound and Vibration 374 (2016) 172–184.

[22] B. Mace, Wave reflection and transmission in beams, J. Sound Vib. 97 (2) (1984) 237–246.

[23] C. Vemula, A. Norris, G. Cody, Attenuation of waves in plates and bars using a graded impedance interface at edges, Journal of Sound and Vibration 196 (1) (1996) 107–127.